

Pathways for Ethanol Dehydrogenation and Dehydration Catalyzed by Ceria (111) and (100) Surfaces

Ariana Beste^{*,†,‡} and Steven H. Overbury[¶]

*Joint Institute for Computational Sciences, The University of Tennessee, Oak Ridge, TN 37831,
Center for Nanophase Materials Sciences, Oak Ridge National Laboratory, Oak Ridge, TN
37831, and Chemical Sciences Division, Oak Ridge National Laboratory, Oak Ridge, TN 37831*

E-mail: bestea@ornl.gov; Phone: 865-241-3160

*To whom correspondence should be addressed

†Joint Institute for Computational Sciences, The University of Tennessee, Oak Ridge, TN 37831

‡Center for Nanophase Materials Sciences, Oak Ridge National Laboratory, Oak Ridge, TN 37831

¶Chemical Sciences Division, Oak Ridge National Laboratory, Oak Ridge, TN 37831

Abstract

We have performed computations to better understand how surface structure affects selectivity in dehydrogenation and dehydration reactions of alcohols. Ethanol reactions on the (111) and (100) ceria surfaces were studied starting from the dominant surface species, ethoxy. We used DFT (PBE+U) to explore reaction pathways leading to ethylene and acetaldehyde and calculated estimates of rate constants employing transition state theory. To assess pathway contributions, we carried out kinetic analysis. Our results show that intermediate and transition state structures are stabilized on the (100) surface compared to the (111) surface. Formation of acetaldehyde over ethylene is kinetically and thermodynamically preferred on both surfaces. Our results are consistent with temperature programmed surface reaction and steady-state experiments, where acetaldehyde was found as the main product and evidence was presented that ethylene formation at higher temperature originates from changes in adsorbate and surface structure.

Keywords: acetaldehyde, ethylene, DFT, transition state theory, rate constant, kinetic analysis

Introduction

Cerium is one of the most abundant rare earth elements with wide applicability in its oxidized form. The most important technological utilization of cerium oxide is the use as a promoter in three-way catalysts to reduce toxic automotive gas emissions.¹ Ceria is capable of storing and releasing oxygen while the oxidation state of cerium changes between +4 and +3. This also enhances catalytic activity when ceria is used as support for transition metals, for instance for the water-gas-shift reaction and steam reforming of hydrocarbons.² Ceria-zirconia supported catalysts have been efficient in other hydrogen forming processes³ as well, such as autothermal reforming, catalytic partial oxidation, dry reforming, and thermochemical water-splitting.⁴ Further, the redox properties of ceria have been exploited to manufacture electrodes in solid oxide fuel cells.¹ Recent developments in the controlled synthesis of nanostructured ceria give rise to exciting new applications, for instance as biomedical protection agents against radiation damage and inflammation.⁵

Most computational studies on ceria and ceria catalyzed reactions⁶ utilize density functional theory (DFT). While fully oxidized ceria does not pose a particular problem for DFT, the presence of Ce^{3+} causes difficulties due to the self-interaction error inherent to density functionals that implement approximate gradient-corrected exchange potentials. Nevertheless, ceria has become a computationally well studied system.⁶ The tendency of gradient-corrected functionals to delocalize atomic-like 4f electrons can be overcome by introducing on-site correlation using a Hubbard-type U term or adding Hartree-Fock exchange in hybrid functionals. The correct description of both the oxidized and reduced states is essential to study technologically important catalytic reactions such as the oxidation of CO to CO_2 or the reduction of NO_x to N_2 over ceria surfaces, which involve oxygen vacancy formation.

In our current work, we examine ethanol dehydrogenation on the fully oxidized (111) and (100) surfaces using DFT. This was motivated by a recent study of the effect of surface structure on the catalytic selectivity for ethanol oxidation over ceria nanocrystals.⁷ In particular, temperature-programmed surface and steady-state reactions with co-fed O_2 were performed using cube, octahedron, and rod shaped nanocrystals as catalysts. Oxygen serves as a healing agent for potentially

formed vacancies on the ceria surfaces. Whereas (100) crystallographic planes are exposed on cubes, octahedra show (111) surfaces, and rods display a mixture of faces. It was postulated that the observed variations in selectivity towards ethylene and acetaldehyde production are a consequence of different rates for α - and β -H-C bond scission on the (111) and (100) surfaces; i.e. reaction occurs on the terrace and not on the edge sites. We, therefore, carry out model surface calculations to investigate the selectivity of acetaldehyde versus ethylene formation from ethanol on the (111) and (100) ceria surfaces.

Computational work on related systems has been conducted previously; notably, the study of ethanol dehydrogenation on the Rh/CeO₂(111) system,⁸ where reported reaction paths proceed through an oxametallacycle involving the Rh atom, and the investigation of acetaldehyde conversion on the ceria (111) surface.⁹ Computational results on ethanol's smaller homolog, methanol, are also available including DFT calculations on the dissociative adsorption on the (111) surface^{10,11} and kinetic data for initial bond-breaking on the (110) surface.¹² Other relevant work includes DFT studies on formaldehyde adsorption^{13,14} and oxidation.¹⁴

In the following we present reaction path and kinetic analysis for acetaldehyde and ethylene formation from ethoxy. The latter is the dominant surface species after ethanol adsorption on the (111) and (100) ceria surfaces.⁷

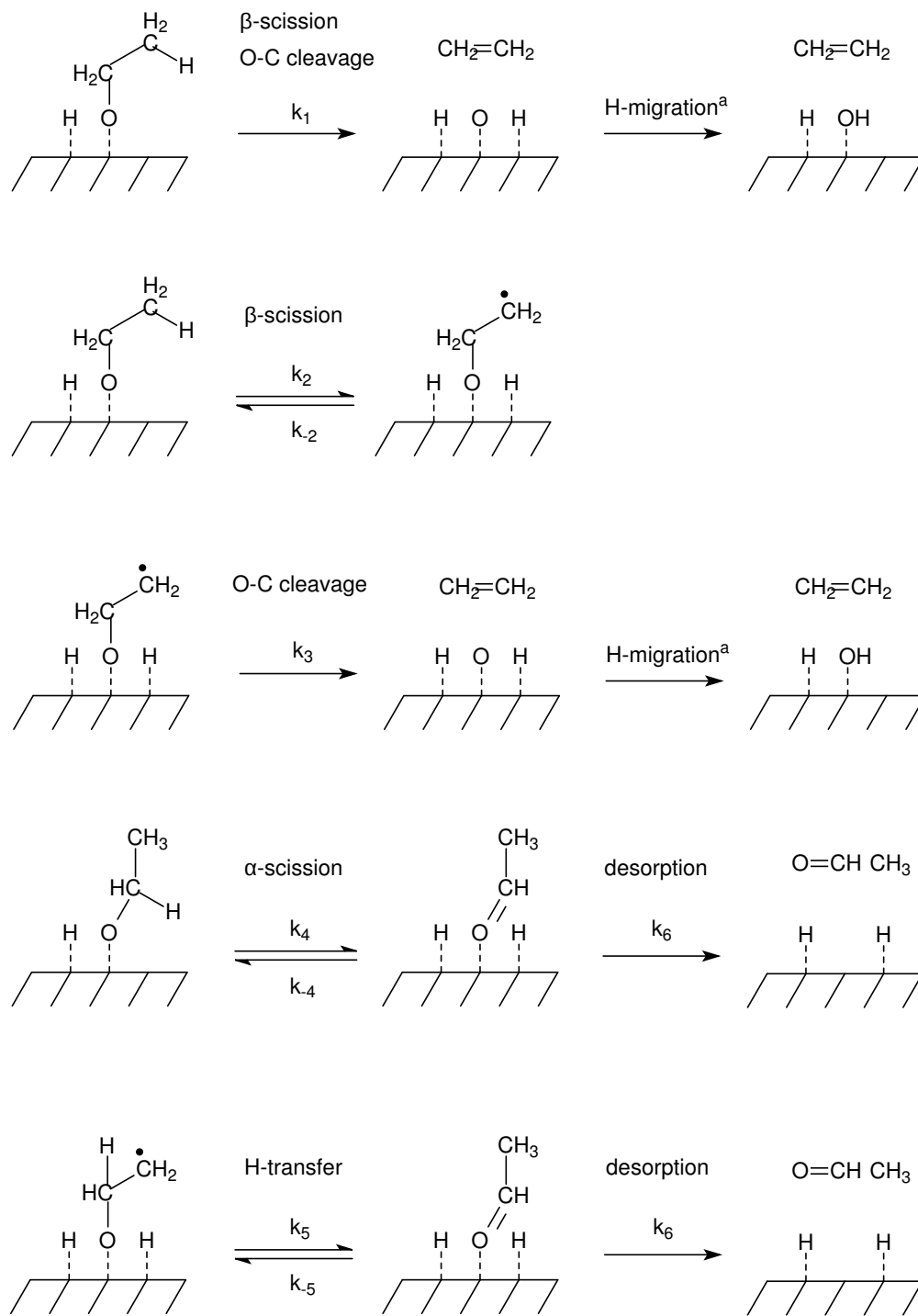


Figure 1: Competitive reactions of ethoxy to form acetaldehyde and ethylene over ceria surfaces studied herein; ^a on (111) surface only.

Computational Details

All electronic structure calculations were carried out using the projector-augmented wave (PAW) method^{15,16} as implemented in the VASP ab initio simulation package.^{17–20} Although we investigated ethoxy dehydrogenation on fully oxidized surfaces, see Figure 1, the overall oxidation state of the carbon atoms in the adsorbate increases during acetaldehyde formation and we, therefore, expected a corresponding reduction of the surface. As discussed above, for the reduced ceria surface standard gradient-corrected exchange-correlation functionals are known to fail and we used the PBE+U^{21,22} functional within the DFT formalism. While a value of 5 eV for U is optimized to position occupied Ce 4f states about 1.3 eV above the oxygen 2p states in bulk Ce₂O₃²³ and is often used in calculations of reduced ceria,⁶ a value of 2–3 eV for U was suggested for the description of redox chemistry over ceria²⁴ and bulk reduction energies,²⁵ a value of 2 eV was recommended for activation barriers.⁹ Here, we chose a value of 2.5 eV for the effective U parameter. This resulted in a lattice constant for CeO₂ of 5.48 Å, intermediate between the lattice constants obtained with PBE(U=0) and PBE+U(U=4.5)²⁶ and compared to the experimental value of 5.41 Å.

We employed spin-polarized functionals, an energy cut off of 700 eV, and dipole corrections perpendicular to the surface. Previously,¹¹ we found that a Γ -centered 4-4-4 Monkhorst-Pack k-point mesh is converged to 0.01 eV for bulk calculations. We, therefore, utilized a Γ -centered 4-4-1 Monkhorst-Pack k-point mesh for the surface calculations.

The (111) ceria surface is oxygen terminated^{27,28} and the most stable surface of ceria. The surface cell was constructed by stacking three units of oxygen-cerium-oxygen layers for a total of 9 atomic layers, which resulted in a zero dipole moment normal to the surface. The top 6 atomic layers were relaxed during optimization, while the bottom 3 layers were fixed. Figure 2 shows the top view of the (111) surface. Using a vacuum layer of 15 Å, we calculated a surface energy of 0.70 J/m² (unrelaxed 0.71 J/m²), similar to the previously published surface energy of 0.71 J/m² using PBE+U(U=5) and 12 atomic layers.²⁹

In contrast to the (111) surface, the (100) surface has a nonzero dipole moment normal to the surface. Experimental observations^{28,30,31} suggest that the (100) surface is terminated by 0.5 ML

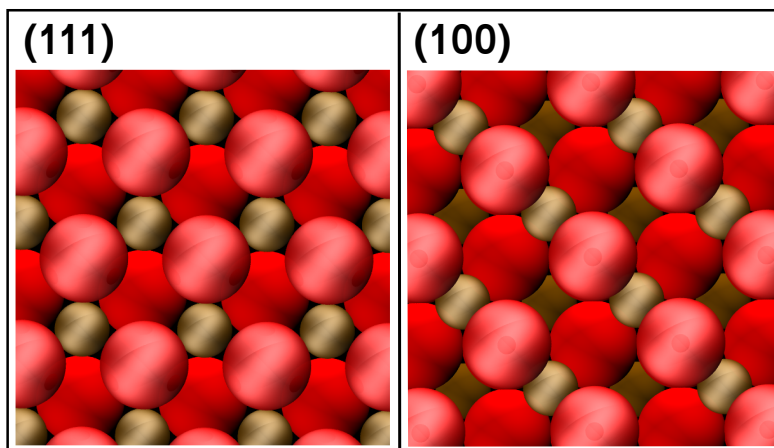


Figure 2: Top views of the (111) surface (left) and the (100) surface (right); top oxygen and cerium layers shown in lighter colors; Ce: ochre, O: red.

(mono layer) of oxygen. To obtain a consistent model, we constructed the oxygen terminated (100) surface by removing half of the oxygen atoms on the surface and adding them at the bottom of the slab in a checker board $[c(2 \times 2)]$ structure, which was found to be most stable³² and is depicted in Figure 2. We again used a surface cell that included 9 atomic layers, where 6 layers were relaxed while the bottom layers were fixed, with a vacuum layer of 15 Å. Surface energies reported in the literature utilizing different functionals and slab thicknesses^{29,32,33} are 2.05 and 2.06 J/m² for the unrelaxed slab and 1.41 - 1.44 J/m² for the relaxed surface, where both sides of the slab were relaxed. This is consistent with our values of 2.09 J/m² for the unrelaxed and 1.76 J/m² for the relaxed surface, where only one side of the slab was relaxed. To ensure that 9 atomic layers are sufficient, we repeated the calculation of the surface energy using a slab with a thickness of 13 atomic layers and obtained a value of 1.75 J/m² for the relaxed surface.

After ethanol adsorption on the ceria surface, the dominant surface species is ethoxy, as found previously from UHV studies of CeO₂(111)³⁴ and for CeO₂ octahedra.⁷ At temperatures where ethylene and acetaldehyde formation occurs⁷ (higher than 250°C on ceria cubes and octahedras), ethanol is present on the surface predominantly in its dissociated form and we, therefore, used ethoxy as the starting point for our calculations. Full coverage of ethoxy on CeO₂(111) was reported to be about 8 nm⁻¹ at 200 K.³⁴ Here, we assumed approximately 1/4 ML coverage or one ethoxy per $p(2 \times 2)$ expansion of the surface cell corresponding to 1.9 and 1.6 nm⁻¹ on the (111) and

(100) surface, respectively. We also assumed that the ethanol H stays co-adsorbed on the surface, thereby avoiding charge separation.

Minimum adsorbate structures were obtained by relaxation of the adsorbate and 6 surface layers. Minimum energy paths were preoptimized with the nudged elastic band method³⁵ (NEB) and transition states were located with the climbing image nudged elastic band method³⁶ (CI-NEB), where we used tools provided by the Henkelman group to set up the input. During the NEB and CI-NEB calculations only the adsorbate and the surface O and Ce atoms that interact directly with the adsorbate were relaxed while most of the surface was fixed. The final geometries of the transition states were recalculated by letting the remainder of the top 6 surface layers relax. Stationary points on the potential energy surface were confirmed by frequency analysis. In a few instances, we found spurious imaginary frequencies, which could not be removed by tight convergence criteria for forces (0.01 eV/Å). In these cases, we displaced along the spurious imaginary mode to find the corresponding minimum along that mode.

Rate constants for surface reactions (k_{react}) were calculated using transition state theory. The harmonic approximation was invoked to compute pre-factors, where only the adsorbate was considered,

$$k_{react} = \frac{kT}{h} \frac{q_{vib}^{TS}}{q_{vib}^R} e^{-\frac{E_a}{kT}}, \quad (1)$$

where k is the Boltzmann constant, h the Planck constant, T the temperature, q_{vib}^{TS} the vibrational partition function of the transition state, and q_{vib}^R the vibrational partition function of the reactant. Although we did not calculate equilibrium constants (K) for thermal equilibria between surface species, we give the formula here so the reader can follow the argument in the text below,

$$K = \frac{q_{vib}^P}{q_{vib}^R} e^{-\frac{\Delta E}{kT}}, \quad (2)$$

where q_{vib}^P is the vibrational partition function of the product and ΔE the energy difference between product and reactant. Desorption rate constants (k_{des}) were calculated employing the model of indirect desorption,³⁷ where the transition state for desorption is free to move across the surface

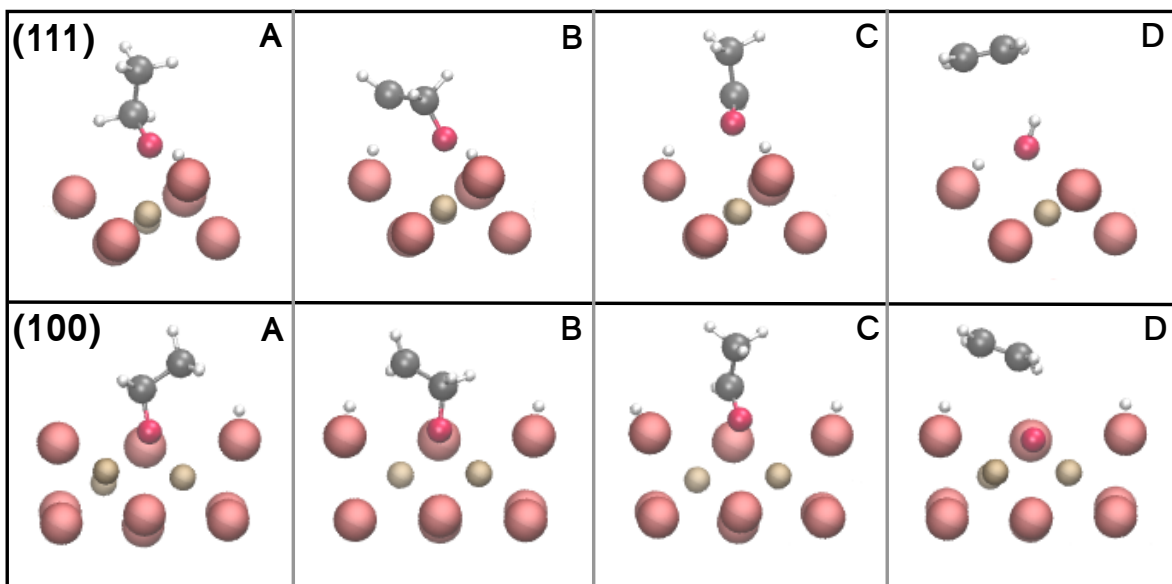


Figure 3: Energetically lowest structures of **A** ethoxy, **B** intermediate, **C** acetaldehyde product, **D** ethylene product, upper panel on the (111) surface, lower panel on the (100) surface; Ce: ochre, O: red, C: gray, H: white.

while rotating and vibrating.

$$k_{des} = \frac{kT}{h} \frac{q_{trans}^{2D,g} q_{rot}^g q_{vib}^g}{q_{vib}^R} e^{-\frac{E_d}{kT}}, \quad (3)$$

where $q_{trans}^{2D,g}$ is the two-dimensional translational partition function, q_{rot}^g the rotational partition function, and q_{vib}^g the vibrational partition function of the desorbed molecule, E_d is the desorption energy.

Kinetic simulations were performed with Mathematica.³⁸ Transition state estimates for rate constants were used in the rate equations that describe the mechanism shown in Figure 1. The corresponding system of coupled differential equations was solved for numerically.

Bader charge analysis was carried out with the code provided by the Henkelman group.^{39–41}

Results and Discussion

Only monodentate ethoxy adsorbed on top a Ce⁴⁺ cation site was found as a stable surface species on the (111) surface. We performed geometry optimizations using 8 different starting structures, where ethoxy can be characterized as standing up with the C-C axis close to perpendicular to

Table 1: Dissociative adsorption energies (relative to the ethanol/ceria system) of ethoxy and adsorption energy (hydrogen atoms are co-adsorbed) of acetaldehyde in eV on the (111) and (100) ceria surfaces.

species		surface	
		(111)	(100)
ethoxy	on top	0.62	0.57
	bidentate	-	1.48
acetaldehyde		0.04	0.21

the surface and laying down with the C-C axis close to parallel to the surface. Further, rotation of ethoxy around the O-Ce axis was considered. The energetically lowest structure is depicted in Figure 3. On the (100) surface, in addition to the monodentate, on-top position, the ethoxy oxygen can also occupy the position of the lattice oxygen that has been removed from the surface layer, yielding a bidentate surface species. We carried out optimizations using 18 different starting structures. The energetically lowest ethoxy structure is the bidentate species shown in Figure 3. The dissociative adsorption energies (relative to the ethanol/ceria system) for the on-top position on the (111) and (100) surface are 0.62 and 0.57 eV, respectively, while the bidentate ethoxy species on the (100) surface is considerably more stable with a dissociative adsorption energy of 1.48 eV (see Table 1). Note, that the dissociative adsorption energy for ethanol in the on-top position appears to be underestimated since it corresponds to a weak interaction between molecule and surface,⁴² while experiment has found ethoxy to be stable on the surface.³⁴ This can be partly attributed to dispersion effects that are not properly accounted for in density functionals.⁶ However, in a study of water on the ceria (111) surface,²⁶ adding dispersion terms to the PBE functional (optPBE-vdW+U) increased adsorption energies only by 0.1 - 0.2 eV.

The energetically lowest ethoxy structures on either surface were used as starting points to locate product and intermediate structures. In particular, we looked for cyclic intermediates but could not find any. The formation of acetaldehyde only involves α -H-C scission, while two bonds have to be broken to yield ethylene, in a one- or two-step process. We found an intermediate ($\text{CH}_2\text{CH}_2\text{O}$), where β -H-C scission occurs first, which is followed by O-C cleavage to obtain ethylene. In addition, intra-molecular H-transfer in the intermediate is an alternative route to ac-

Table 2: Sum of Bader atomic charges of surface species in electrons (including H and O atoms on surface); magnetic moments of second layer cerium atoms, numbering according to Figure 4.

surface	species	charge	magnetic moment [μ_B]			
			Ce(1)	Ce(2)	Ce(3)	Ce(4)
(111)	ethoxy	0.09	0.00	0.00	0.00	0.00
	intermediate	0.59	-0.02	-0.76	-0.02	-0.03
	acetaldehyde	1.16	-0.43	0.56	0.83	0.01
	ethylene	0.27	0.00	0.00	0.00	0.00
(100)	ethoxy	0.06	0.00	0.00	0.00	0.00
	intermediate	0.58	0.00	0.80	0.22	0.00
	acetaldehyde	1.14	0.03	0.79	0.78	0.01
	ethylene	0.25	0.00	0.00	0.00	0.00

etaldehyde formation. While we were able to locate acetaldehyde adsorbed on the surface, ethylene does not form a stable adsorption product on the ceria surface but desorbs immediately. Surface hydrogen readily moves towards the oxygen atom left behind on the (111) surface during ethylene formation yielding a hydroxy bound to the surface. A NEB calculation indicated that there is no activation barrier for this process. On the (100) surface H-migration to the oxygen atom does not provide stabilization since the latter is fully integrated in the top oxygen layer of the surface. The competitive reactions of ethoxy over ceria to yield acetaldehyde and ethylene studied herein are summarized in Figure 1.

On the (111) surface, ethoxy is surrounded by 3 surface oxygen atoms. One of them carries the co-adsorbed ethanol H and the other two are equivalent and free to accept H from either α - or β -H-C scission. On the (100) surface, ethoxy possesses 4 neighboring surface oxygen atoms. Again, one of them is occupied. We place the α - or β -H opposite to the occupied site. Although the other adjacent O atoms are not completely equivalent, H transfer pathways to these are expected to be similar and not explored herein. Product and intermediate structures are given in Figure 3. We only considered reaction paths to products present immediately after reaction. In particular, a more stable, chemisorbed species of acetaldehyde exists on the (111) ceria surface.⁹ While we incorporate desorption in the kinetic analysis later on, product rearrangement and further reactions were not included in this work.

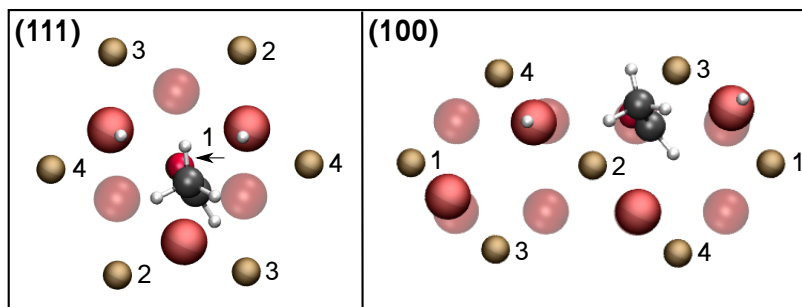


Figure 4: Top view of acetaldehyde products on the (111) and (100) surface; 3 surface layers are shown, the lowest O layer is transparent, second layer Ce atoms numbered; Ce: ochre, O: red, C: gray, H: white.

In order to analyse the degree of reduction of cerium that occurs during reaction (see Figure 1), we calculated Bader atomic charges, local magnetic moments, and projected densities of states (PDOS). Table 2 includes the sum of the Bader atomic charges of the adsorbates. A positive value indicates that an equal amount of negative charge has been transferred to the surface. For a better comparison between the (111) and the (100) surface, the (111) ethylene product included in the table is the minimum structure prior to H migration to form OH. The Bader charge analysis shows very similar charge transfer on the (111) as on the (100) surfaces. Ethoxy combined with ethanol H is close to charge neutral, indicating that no charge transfer to the surface takes place. When the intermediate is formed, the sum of the carbon oxidation states formally changes from -4 to -3, potentially releasing one electron to the surface. Charge analysis indeed shows a charge transfer to the surface of 0.59 electron on the (111) surface and 0.58 electron on the (100) surface. The sum of the formal oxidation states of the two carbon atoms in acetaldehyde is -2, giving the possibility for two electrons to be transferred to the surface. We observe that 1.16 and 1.14 electrons are donated from the acetaldehyde to the (111) and (100) surface, respectively, approximately twice as much charge as from the intermediate. Although the overall oxidation state in ethylene is with -4 the same as in ethoxy, a formally doubly negative oxygen ion is produced on the surface giving rise to a fairly small amount of charge transfer to the surface.

The magnetic moments of the second layer cerium atoms shown in Table 2 indicate if the cerium atoms are reduced. However, the degree of 4f electron localization is a function of the pa-

parameter U and one should be cautious when interpreting the sites of nonzero magnetic moment.⁴³ Similar can be said about the analysis of the projected density of states (PDOS) below. Cerium atoms are numbered according to Figure 4. Reduction of second layer cerium atoms with varying degree of delocalization can be observed in the intermediates and the acetaldehyde products on both surfaces in agreement with the results of the charge analysis. Ethoxy does not reduce cerium and there is also no magnetic moment on the cerium atoms of the ethylene products. The reduction of cerium in the intermediates is accompanied by a magnetic moment on the β -carbon atom of $0.27 \mu_B$ and $0.28 \mu_B$ on the (111) and (100) surface, respectively, showing the radical character of the β -carbon. The unpaired spin density in the acetaldehyde products is considerably larger than in the intermediates, again signifying that the surface is further reduced in the acetaldehyde product in accordance with the charge analysis.

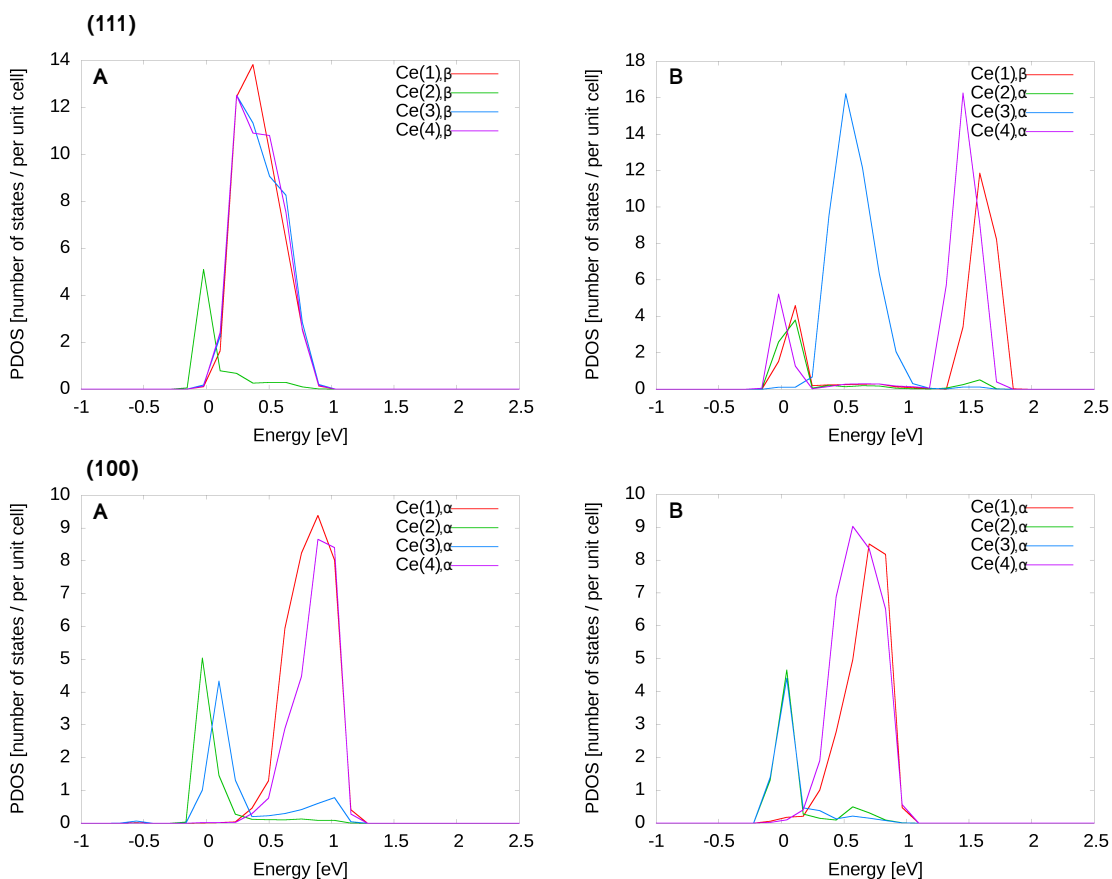


Figure 5: Projected densities of states: 4f states of the second layer cerium atoms, numbering according to Figure 4; **A** - intermediate, **B** - acetaldehyde product, upper panel on the (111) surface, lower panel on the (100) surface.

In addition, we monitored PDOS for the 4f states of the second layer cerium atoms. The 4f states are unoccupied when ethoxy is adsorbed and in the ethylene product. Partial occupation of the 4f states is observed for the intermediate and the acetaldehyde product; the corresponding PDOS are given in Figure 5. The PDOS mirror the magnetic moments in Table 2: a negative magnetic moment corresponds to a partial occupation of the β -spin 4f states, while a positive magnetic moment correlates with a partial occupation of the α -spin 4f states of that cerium atom. Note, however, that the degree of splitting of the 4f states due to cerium reduction is a function of the parameter U.⁴³

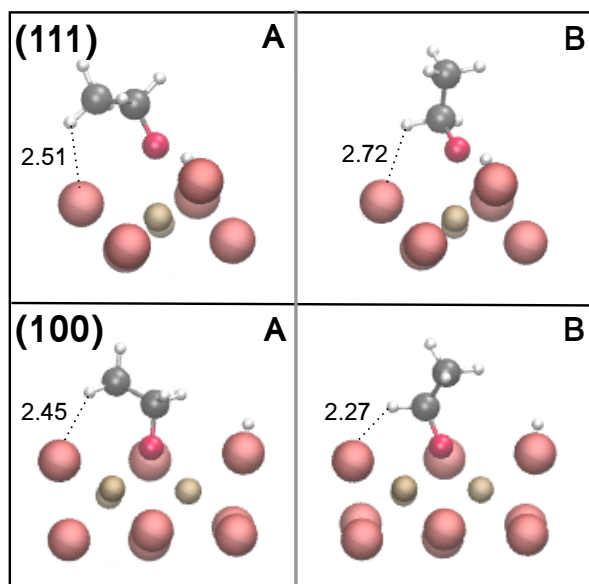


Figure 6: Initial ethoxy structure for **A** β -H-C scission, **B** α -H-C scission, upper panel on the (111) surface, lower panel on the (100) surface; O-H distances in Å; Ce: ochre, O: red, C: gray, H: white.

The lowest energy structures for dissociatively adsorbed ethanol on the (111) and (100) surface are given in Figure 3. For α - or β -H abstraction to occur, the respective H atom has to be in close proximity to the surface oxygen to which the H atom is transferred to. This can be easily accommodated by a rotation or tilting of ethoxy around the O-C axis. The resulting minimum structures are shown in Figure 6 and are very close in energy. We expect that the transitions between the structures proceed through correspondingly small barriers. We performed a CI-NEB calculation for the rotation of ethoxy on the (111) surface yielding the reactant for β -H abstraction

(Figure 6, **B** upper panel) and did not find a barrier. We, therefore, assumed that the rotamers are in thermodynamic equilibrium with each other. For α -H abstraction on the (111) surface, a rotation is not necessary because the energetically lowest ethoxy is oriented such that α -H transfer can occur.

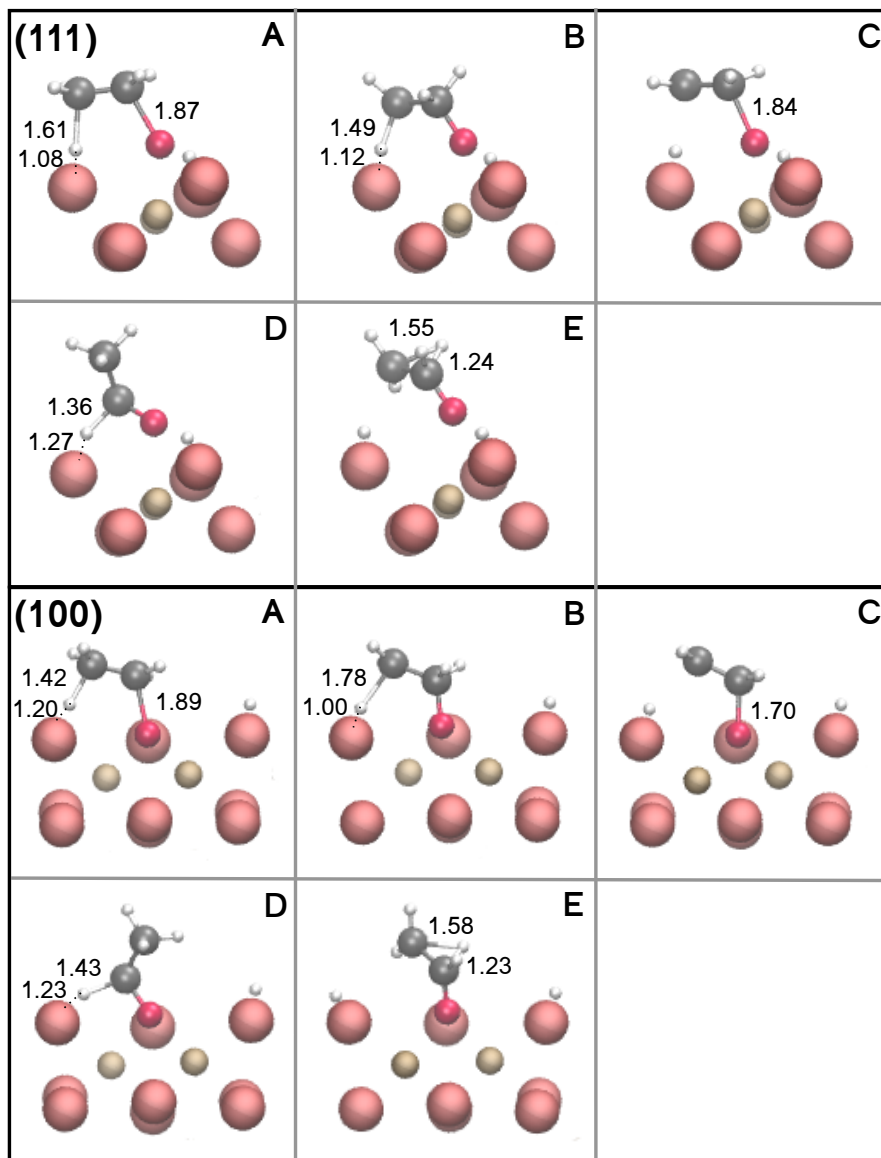


Figure 7: Transition states for **A** β -H-C scission and simultaneous O-C cleavage, **B** β -H-C scission, **C** O-C cleavage, **D** α -H-C scission, **E** intramolecular H transfer, upper panel on the (111) surface, lower panel on the (100) surface; distances of transitioning bonds in Å; Ce: ochre, O: red, C: gray, H: white.

We located transition states on the (111) and (100) surface for the one-step ethylene formation involving β -H transfer to the surface and simultaneous O-C cleavage, intermediate generation

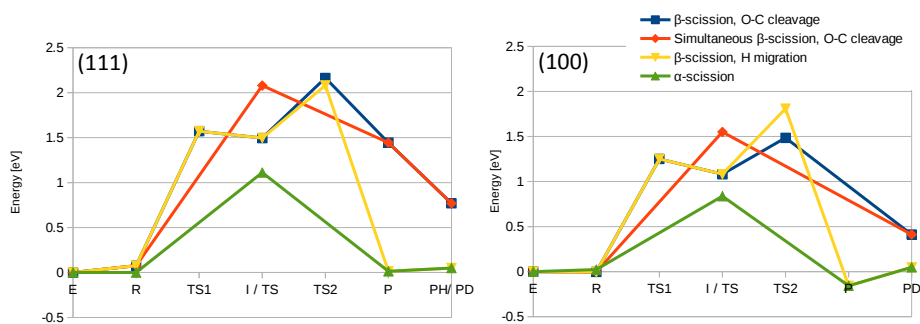


Figure 8: Reaction profiles for ethylene and acetaldehyde formation on the (111) and (100) surface; E - ethoxy, R - rotated/tilted ethoxy, TS1, TS, TS2 - transition states, I - intermediate, P - product, PH - product with migrated H (ethylene product), PD - desorbed product.

through β -H abstraction, intermediate reaction to ethylene via O-C cleavage, intermediate transformation to acetaldehyde through intramolecular H-transfer, and α -H transfer to the surface to form acetaldehyde. The transition states are depicted in Figure 7 and the corresponding reaction profiles in Figure 8. Note that reaction energies and barriers in Figure 8 are given relative to the ethoxy/ceria system with ethoxy in its lowest energy conformation as shown in Figure 3 and can be found in tabular form in the Supporting Information. We observe that transition states and intermediate are stabilized on the (100) compared to the (111) surface. The transition state for intramolecular H-transfer, which does not directly involve the ceria surface, is notably less stabilized. Pathways for stepwise and simultaneous β -H-C scission and O-C cleavage leading to ethylene are close in energy on both surfaces. Intramolecular H-transfer on the (111) surface has nearly the same barrier as O-C cleavage after intermediate formation and is only 0.32 eV higher than on the (100). Acetaldehyde formation through α -H-C scission is on both surfaces the energetically lowest reaction path. Even though we located a minimum structure for acetaldehyde adsorbed on the (111) surface, the adsorption energy is very small. On the (100) surface the (dipole corrected) adsorption energy of acetaldehyde is 0.21 eV (see Table 1).

To obtain selectivities for acetaldehyde and ethylene formation at finite temperature including all identified pathways and subsequent acetaldehyde desorption, we calculated rate constants for each elementary step and simulated reaction progress. Rate constant estimates at 300°C and 450°C are given in Table 3 and corresponding prefactors can be found in the Supporting Information. Note that we used a symmetry number of two for H-C scission on the (111) surface since there

Table 3: Rate constant estimates k for elementary steps shown in Figure 1 and included in the kinetic analysis, subscript (s) indicates surface species and (g) gas phase.

label	elementary reaction step	$k [s^{-1}]$			
		(111) surface		(100) surface	
		300° C	450° C	300° C	450° C
k_1	$CH_3CH_2O_{(s)} \rightarrow CH_2CH_2_{(g)} + H_{(s)} + O_{(s)}$	2×10^{-4}	6×10^{-1}	4×10^1	2×10^4
k_2	$CH_3CH_2O_{(s)} \rightarrow CH_2CH_2O_{(s)} + H_{(s)}$	6	2×10^3	4×10^3	6×10^5
k_{-2}	$CH_2CH_2O_{(s)} + H_{(s)} \rightarrow CH_3CH_2O_{(s)}$	3×10^{12}	3×10^{12}	1×10^{11}	3×10^{11}
k_3	$CH_2CH_2O_{(s)} \rightarrow CH_2CH_2_{(g)} + O_{(s)}$	1×10^7	2×10^8	1×10^9	7×10^9
k_4	$CH_3CH_2O_{(s)} \rightarrow CH_3CHO_{(s)} + H_{(s)}$	1×10^5	8×10^6	1×10^7	3×10^8
k_{-4}	$CH_3CHO_{(s)} + H_{(s)} \rightarrow CH_3CH_2O_{(s)}$	2×10^2	1×10^4	1×10^4	5×10^5
k_5	$CH_2CH_2O_{(s)} \rightarrow CH_3CHO_{(s)}$	7×10^8	7×10^9	2×10^8	3×10^9
k_{-5}	$CH_3CHO_{(s)} \rightarrow CH_2CH_2O_{(s)}$	4×10^{-6}	2×10^{-2}	1×10^{-2}	3×10^1
k_6	$CH_3CHO_{(s)} \rightarrow CH_3CHO_{(g)}$	8×10^{14}	4×10^{14}	3×10^{14}	3×10^{14}

are two equivalent surface O available (one surface O is occupied by co-adsorbed ethanol H). On the (100) surface there are three surface O closest to the adsorbate and free to accept H, the symmetry number is three. Note, however, that the co-adsorbed H breaks the symmetry and the three pathways may differ to some extent. In addition, we introduced symmetry numbers for the varying number of equivalent H atoms in the reactants and the intermediate. Also note that if we assume that rotated and tilted ethoxy structures on the surface are in thermal equilibrium with the energetically lowest ethoxy structure, the transition state rate constants for the combined equilibrium and forward reactions equal the rate constants where the lowest ethoxy structure is the reactant. This is because the partition functions of the higher energy structures cancel and the barrier is adjusted by the energy differences of the ethoxy structures.

We performed kinetic analysis by integration of the coupled rate equations corresponding to the elementary steps contained in Table 3 and Figure 1. The starting point of our simulations was ethoxy adsorbed on the surface. We chose a unit of $\mu\text{mol}/\text{m}^2/\text{s}$ for the rate of reaction. The initial coverage is then $3 \mu\text{mol}/\text{m}^2$ (approximately 2 ethoxy per nm^2) and the amount of product formed is understood as the number of μmol of product formed per m^2 of surface. Once a product is released in the gas stream back reaction is not allowed. In a temperature-programmed surface reaction (TPSR) and steady-state reaction, the reaction mixture over the surface is a constantly flowing gas

stream and, ideally, products are removed and detected as they are formed.⁷ In practice, products released in the gas stream may re-adsorb at a later time, this is neglected here. The simulation result for ethylene and acetaldehyde formation on the (111) and (100) ceria surface at 300° C and 450° C is that acetaldehyde is almost exclusively produced. Figure 9 shows, as an example, reaction progress as a function of time on the (111) surface at 300° C. Note, that even at the scale where ethylene formation becomes visible (right side of Figure 9), the intermediate does not accumulate and almost all of the acetaldehyde desorbs immediately. The calculated selectivity at steady state for acetaldehyde over ethylene formation ranges from 7×10^8 [(111), 300° C], 1×10^7 [(111), 450° C], 2×10^5 [(100), 300° C] to 8×10^3 [(100), 450° C]. Although, the selectivity is smaller on the (100) surface, ethylene formation is not competitive on either surface. Also temperature increase within the experimental range does not lead to a prediction of an appreciable amount of ethylene production. In TPSR experiments,⁷ acetaldehyde is indeed predominantly observed at 300° C. Also steady-state reaction experiments at 350° C do not show a significant amount of ethylene being formed. In TPSR experiments at 450° C, ethylene production is competitive over octahedra-shaped ceria nanoparticle, which expose the (111) surface, and dominates on cube-shaped ceria nanoparticles, which are terminated by (100) surfaces. Our calculations do not show that ethylene production from ethoxy is favourable either kinetically nor thermodynamically and, therefore, a raise in temperature does not lead to ethylene being the main product. However, the increased detection of ethylene at higher temperature in TPSR experiments was proposed to occur in an anaerobic regime, where dominant surface species and surface structure (for instance through vacancy formation) might change and a different mechanism for ethylene production may apply.⁷ Our work supports the hypothesis that ethylene at higher temperature is not formed from ethoxy on the fully oxidized surface.

We also analysed the contribution of the two-step pathways through intermediate formation. While it is negligible for acetaldehyde production, one- and two-step pathways have equal weight for ethylene formation on the (100) surface. On the (111) surface, the one-step pathway leading to ethylene is preferred with a selectivity of 8 at 300° C and 5 at 450° C.

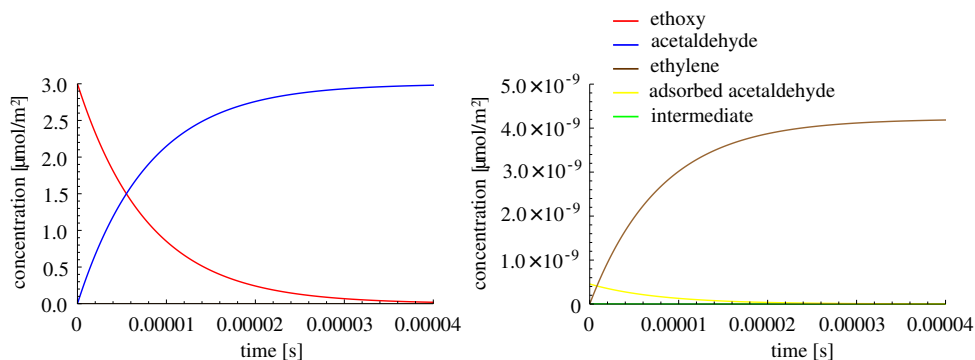


Figure 9: Reactant depletion and product formation as a function of time on the (111) surface at 300° C, left: reaction progress, right: same as left but focused in on low concentration region.

At this point, we would like to advise against the use of the rate constant estimates given in Table 3 as absolute values. Although kinetic data obtained with DFT is used in ab initio kinetic Monte Carlo simulations to study chemical kinetics on catalytic surfaces,⁴⁴ the accuracy of DFT is not sufficient to predict absolute rate constants reliably. The self-interaction error in DFT causes a systematic underestimation of energy barriers. This error is exaggerated in rate constant calculations due to the exponential dependence of the rate constant on the activation energy. For instance, an underestimation of the barrier of 0.5 eV causes the rate constant at 300° to decrease by 4 orders of magnitude. It is difficult to gauge the error made in reaction barriers but using the DFT+U method, errors far greater than 0.5 eV have been reported for the heat of reduction and defect formation energies.⁶ Hybrid functionals correct the self-interaction error to some extent but are prohibitively expensive for our systems, especially for reactions on the (100) surface. The large discrepancy of a few orders of magnitude between the calculated rate of reaction (initial slope in Figure 9 is approximately $3 \times 10^5 \mu\text{mol}/\text{m}^2/\text{s}$ at 300°C) and experimental reactivity ($4 \times 10^{-1} \mu\text{mol}/\text{m}^2/\text{s}$ for octahedra at 350°C in⁷) can also be caused by adsorbates other than ethoxy being on the surface, which would slow reaction. The presence of additional surface species was apparent in the DRIFT spectra in.⁷ We used calculated rate constants to obtain an understanding of pathway selectivity, given our computed values for reaction barriers.

Conclusion

Ethoxy is the dominant surface species when ethanol is adsorbed on ceria surfaces. We performed PBE+U (U=2.5eV) calculations to explore reaction pathways of ethoxy on fully oxidized (111) and (100) ceria surfaces yielding ethylene and acetaldehyde. We calculated estimates for rate constants using transition state theory and carried out kinetic simulations to assess the relative pathway contributions. We identified a one-step pathway for ethylene formation, where β -H transfer occurs simultaneously with O-C bond scission, and a two-step pathway, where β -H transfer occurs first leading to an intermediate that further reacts through O-C scission. This intermediate can also intramolecularly transfer a hydrogen atom producing acetaldehyde. The latter pathway and both ethylene pathways are higher in energy than the one-step pathway for acetaldehyde formation, where the α -H is transferred to the surface. Bader charge analysis, projected density of states, and magnetic moments of the reactant and products show that cerium becomes partially reduced during acetaldehyde formation, while it remains fully oxidized during ethylene production. At 300° C, the only appreciable product on both surfaces is acetaldehyde. Ethylene formation is neither kinetically nor thermodynamically preferred and a temperature increase to 450° C does not lead to a reverse selectivity, where ethylene is the main product. Our results agree with temperature-programmed surface and steady-state reaction experiments, where an ethanol/oxygen stream was flowed over ceria nanoparticles at 300° C and 350° C and the dominant product was found to be acetaldehyde. Experimental evidence led to the hypothesis that ethylene formation seen at 450° C does not originate from ethoxy on the oxidized surface but is produced in a regime where adsorbates and surface have significantly changed. Our results support this hypothesis.

Acknowledgements

This research was sponsored by the Division of Chemical Sciences, Geosciences, and Biosciences, Office of Basic Energy Sciences, U.S. Department of Energy. The computational part of this project was conducted at the Center for Nanophase Materials Sciences under a user proposal.

The Center is sponsored at Oak Ridge National Laboratory by the Scientific User Facilities Division, Office of Basic Energy Sciences, U.S. Department of Energy. This research was in part supported by an allocation of advanced computing resources provided by the National Science Foundation and performed on Kraken and Darter at the National Institute for Computational Sciences (<http://www.nics.tennessee.edu/>). This research also used resources of the National Energy Research Scientific Computing Center, a DOE Office of Science User Facility supported by the Office of Science of the U.S. Department of Energy under Contract No. DE-AC02-05CH11231.

Supporting Information Available: Supporting information contains prefactors of rate constant estimates, reaction energies and barriers corresponding to Figure 8 in tabular form. This material is available free of charge via the Internet at <http://pubs.acs.org>.

References

- [1] *Catalysis by Ceria and Related Materials*; Trovarelli, A., Ed.; Imperial College Press: London, 2002.
- [2] Gorte, R. J. Ceria in Catalysis: From Automotive Applications to the Water Gas Shift Reaction. *AICHE* **2010**, *56*, 1126 – 1135.
- [3] Nahar, G.; Dupont, V. Hydrogen Production from Simple Alkanes and Oxygenated Hydrocarbons over Ceria-Zirconia Supported Catalysts: Review. *Renew. Sust. Energy Rev.* **2014**, *32*, 777 – 796.
- [4] Abanades, S.; Legal, A.; Cordier, A.; Peraudeau, G.; Flamant, G.; Julbe, A. Investigation of Reactive Cerium-Based Oxides for H₂ Production by Thermochemical Two-Step Water-Splitting. *J. Mater. Sci.* **2010**, *45*, 4163 – 4173.
- [5] Sun, C.; Li, H.; Chen, L. Nanostructured Ceria-Based Materials: Synthesis, Properties, and Applications. *Energy Environ. Sci.* **2012**, *5*, 8475 – 8505.

- [6] Paier, J.; Penschke, C.; Sauer, J. Oxygen Defects and Surface Chemistry of Ceria: Quantum Chemical Studies Compared to Experiment. *Chem. Rev.* **2013**, *113*, 3949 – 3985.
- [7] Li, M.; Wu, Z.; Overbury, S. H. Surface Structure Dependence of Selective Oxidation of Ethanol on Faceted CeO₂ Nanocrystals. *J. Cat.* **2013**, *306*, 164 – 176.
- [8] Chen, H.-L.; Liu, S.-H.; Ho, J.-J. Theoretical Calculation of the Dehydrogenation of Ethanol on a Rh/CeO₂(111) Surface. *J. Phys. Chem. B* **2006**, *110*, 14816 – 14823.
- [9] Calaza, F. C.; Xu, Y.; Mullins, D. R.; Overbury, S. H. Oxygen Vacancy-Assisted Coupling and Enolization of Acetaldehyde on CeO₂(111). *J. Am. Chem. Soc.* **2012**, *134*, 18034 – 18045.
- [10] Mei, D.; Deskins, N. A.; Dupuis, M.; Ge, Q. Methanol Adsorption on the Clean CeO₂(111) Surface: A Density Functional Theory Study. *J. Phys. Chem. C* **2007**, *111*, 10514 – 10522.
- [11] Beste, A.; Mullins, D. R.; Overbury, S. H.; Harrison, R. J. Adsorption and Dissociation of Methanol on the Fully Oxidized and Partially Reduced (111) Cerium Oxide Surface: Dependence on the Configuration of the Cerium 4f Electrons. *Surface Science* **2008**, *602*, 162 – 175.
- [12] Mei, D.; Deskins, N. A.; Dupuis, M.; Ge, Q. Density Functional Theory Study of Methanol Decomposition on the CeO₂(110) Surface. *J. Phys. Chem. C* **2008**, *112*, 4257 – 4266.
- [13] Mei, D.; Deskins, N. A.; Dupuis, M. A Density Functional Theory Study of Formaldehyde Adsorption on Ceria. *Surface Science* **2007**, *601*, 4993 – 5001.
- [14] Teng, B.-T.; Jiang, S.-Y.; Yang, Z.-X.; Luo, M.-F.; Lan, Y.-Z. A Density Functional Theory Study of Formaldehyde Adsorption and Oxidation on CeO₂ (111) Surface. *Surface Science* **2010**, *604*, 68 – 78.
- [15] Blochl, P. E. Projector Augmented-Wave Method. *Phys. Rev. B* **1994**, *50*, 17953 – 17979.
- [16] Kresse, G.; Joubert, D. From Ultrasoft Pseudopotentials to the Projector Augmented-Wave Method. *Phys. Rev. B* **1999**, *59*, 1758 – 1775.

- [17] Kresse, G.; Hafner, J. Ab Initio Molecular Dynamics for Liquid Metals. *Phys. Rev. B* **1993**, *47*, 558 – 561.
- [18] Kresse, G.; Hafner, J. Ab Initio Molecular Dynamics Simulation of the Liquid-Metal-Amorphous-Semiconductor Transition in Germanium. *Phys. Rev. B* **1994**, *49*, 14251 – 14269.
- [19] Kresse, G.; Furthmüller, J. Efficiency of Ab Initio Total Energy Calculations for Metals and Semiconductors Using a Plane-Wave Basis Set. *Comput. Mat. Sci.* **1996**, *6*, 15 – 50.
- [20] Kresse, G.; Furthmüller, J. Efficient Iterative Schemes for Ab Initio Total Energy Calculations Using a Plane-Wave Basis Set. *Phys. Rev. B* **1996**, *54*, 11169 – 11186.
- [21] Perdew, J. P.; Burke, K.; Ernzerhof, M. Generalized Gradient Approximation Made Simple. *Phys. Rev. Lett.* **1996**, *77*, 3865 – 3868.
- [22] Dudarev, S. L.; Botton, G. A.; Savrasov, S. Y.; Humphreys, C. J.; Sutton, A. P. Electron-Energy-Loss Spectra and the Structural Stability of Nickel Oxide: An LSDA+U study. *Phys. Rev. B* **1998**, *57*, 1505 – 1509.
- [23] Watkins, M. B.; Foster, A. S.; Shluger, A. L. Hydrogen Cycle on CeO₂ (111) Surfaces: Density Functional Theory Calculations. *J. Phys. Chem. C* **2007**, *111*, 15337 – 15341.
- [24] Huang, M.; Fabris, S. CO Adsorption and Oxidation on Ceria Surfaces from DFT+U Calculations. *J. Phys. Chem. C* **2008**, *112*, 8643 – 8648.
- [25] Loschen, C.; Carrasco, J.; Neyman, K. M.; Illas, F. First-principles LDA+U and GGA+U study of cerium oxides: Dependence on the effective U parameter. *Phys. Rev. B* **2007**, *75*, 035115–1 – 8.
- [26] Fernández-Torre, D.; Kośmider, K.; Carrasco, J.; Ganduglia-Pirovano, M. V.; Pérez, R. Insight in to the Adsorption of Water on the Clean CeO₂(111) Surface with van der Waals and Hybrid Density Functionals. *J. Phys. Chem. C* **2012**, *116*, 13584 – 13593.

- [27] Mullins, D. R.; Radulovic, P. V.; Overbury, S. H. Ordered Cerium Oxide Thin Films Grown on Ru(0001) and Ni(111). *Surf. Sci.* **1999**, *429*, 186 – 198.
- [28] Wu, Z.; Jiang, D.-e.; Mann, A. K. P.; Mullins, D. R.; Qiao, Z.-A.; Allard, L. F.; Zeng, C.; Jin, R.; Overbury, S. H. Thiolate Ligands as a Double-Edged Sword for CO Oxidation on CeO₂ Supported Au₂₅(SCH₂CH₂Ph)₁₈ Nanoclusters. *J. Amer. Chem. Soc.* **2014**, *136*, 6111 – 6122.
- [29] Molinari, M.; Parker, S. C.; Sayle, D. C.; Islam, M. S. Water Adsorption and Its Effect on the Stability of Low Index Stoichiometric and Reduced Surfaces of Ceria. *J. Phys. Chem. C* **2012**, *116*, 7073 – 7082.
- [30] Herman, G. S. Surface Structure Determination of CeO₂(001) by Angle-Resolved Mass Spectroscopy of Recoiled Ions. *Phys. Rev. B* **1999**, *59*, 14899 – 14902.
- [31] Nörenberg, H.; Harding, J. H. The Surface Structure of CeO₂(001) Single Crystals Studied by Elevated Temperature STM. *Surface Science* **2001**, *477*, 17 – 24.
- [32] Skorodumova, N. V.; Baudin, M.; Hermansson, K. Surface Properties of CeO₂ from First Principles. *Phys. Rev. B* **2004**, *69*, 075401–1 – 8.
- [33] Nolan, M.; Parker, S. C.; Watson, G. W. The Electronic Structure of Oxygen Vacancy Defects at the Low Index Surfaces of Ceria. *Surface Science* **2005**, *595*, 223 – 332.
- [34] Mullins, D. R.; Senanayake, S. D.; Chen, T.-L. Adsorption and Reaction of C₁ – C₃ Alcohols over CeO_x(111) Thin Films. *J. Phys. Chem. C* **2010**, *114*, 17112 – 17119.
- [35] Jónsson, H.; Mills, G.; Jacobsen, K. W. In *Classical and Quantum Dynamics in Condensed Phase Simulations*; Berne, B. J., Ciccotti, G., Coker, D. F., Eds.; World Scientific, 1998; Chapter Nudged Elastic Band Method for Finding Minimum Energy Paths of Transitions, p 385.

- [36] Henkelman, G.; Uberuaga, B. P.; Jónsson, H. A Climbing Image Nudged Elastic Band Method for Finding Saddle Points and Minimum Energy Paths. *J. Chem. Phys.* **2000**, *113*, 9901 – 9904.
- [37] Chorkendorff, I.; Niemantsverdriet, J. W. *Concepts of Modern Catalysis and Kinetics*; Wiley-VCH GmbH & Co. KGaA, 2003.
- [38] *Mathematica*, Version 7.0 ed.; Wolfram Research, Inc.; Champaign, IL, 2008.
- [39] Tang, W.; Sanville, E.; Henkelman, G. A Grid-Based Bader Analysis Algorithm Without Lattice Bias. *Condens. Matter* **2009**, *21*, 084204–1 – 7.
- [40] Sanville, E.; Kenny, S. D.; Smith, R.; Henkelman, G. An Improved Grid-Based Algorithm for Bader Charge Analysis. *J. Comp. Chem.* **2007**, *28*, 899 – 908.
- [41] Henkelman, G.; Arnaldsson, A.; Jónsson, H. A Fast and Robust Algorithm for Bader Decomposition of Charge Density. *Comput. Mater. Sci.* **2006**, *36*, 254 – 360.
- [42] Nolan, M.; Watson, G. W. The Surface Dependence of CO Adsorption on Ceria. *J. Phys. Chem. B* **2006**, *110*, 16600 – 16606.
- [43] Castleton, C. W. M.; Kullgren, J.; Hermansson, K. Tuning LDA+U for Electron Localization and Structure at Oxygen Vacancies in Ceria. *J. Chem. Phys.* **2007**, *127*, 244704–1 – 11.
- [44] Stamatakis, M.; Vlachos, D. G. Unraveling the Complexity of Catalytic Reactions via Kinetic Monte Carlo Simulations: Current Status and Frontiers. *ACS Catal.* **2012**, *2*, 2648 – 2663.

TOC

